Available online at www.sciencedirect.com

ScienceDirect

Mendeleev Commun., 2019, **29**, 400–402

Mendeleev Communications

Synthesis of MOF-derived bimetallic nanocarbons CuNi@C with potential applications as counter electrodes in solar cells

Lizbeth Marroquín Tijerina, Cesar M. Oliva González, Boris I. Kharisov,* Thelma E. Serrano Quezada, Yolanda Peña Méndez, Oxana V. Kharissova and Idalia Gómez de la Fuente

Universidad Autónoma de Nuevo León, 66455 San Nicolás de los Garza, Nuevo León, México.
E-mail: bkhariss@hotmail.com

DOI: 10.1016/j.mencom.2019.07.014

A Cu–Ni-containing bimetallic carbon-based material was prepared by the pyrolysis of a metal-organic framework (MOF) synthesized from copper and nickel salts and trimesic acid precursors at room temperature. This material was tested as a counter electrode for the reduction of I_3^- by means of cyclic voltammetry.

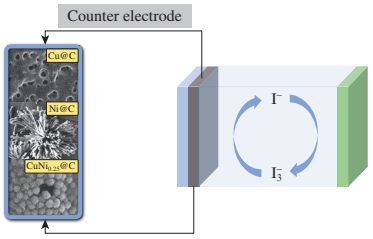

In the context of searching for renewable energy sources, dye-sensitized solar cells (DSSCs) have been widely studied in order to increase their efficiency and reduce the production costs.[1] Therefore, a counter electrode for this kind of solar cells should exhibit high conductivity and high catalytic activity[2] to catalyze iodine electrolyte reduction and recollect electrons.[3–5] For this reason, platinum is commonly used,[6] which increases the cost of DSSCs. The main advantage of DSSCs over other solar cells is their easy manufacture and cost-benefit ratio, however it is necessary to reduce their cost to compete with other solar cells. To solve this problem, the platinum counter electrode can be replaced with materials such as carbon,[7–9] graphene,[10] copper oxide,[11] and composites.[12,13] Among those, MOF-derived carbons seem to be a brilliant choice since the MOF cations become zero-valent after carbonization and loose most of the functional groups coming from a binder. These materials possess a good catalytic activity, high thermal stability and are inexpensive.[14–17] Deok *et al.* improved the electrochemical activity of copper-containing MOFs by the addition of carbon nanotubes.[18] Zheng *et al.* encapsulated FeNi alloy in carbon nanotubes to achieve an electrocatalytic response of DSSCs to the reduction of the triiodide anion [reactions (1),(2)].[19] Sun *et al.* reported the catalytic activity towards the reduction of triodide using nanocarbon obtained by the pyrolysis of ZIF-8 (a MOF based on zinc(II) cations and methylimidazole as a binder).[20–24]

$$I_3^- + 2\bar{e} \rightarrow 3I^- \quad (1)$$

$$3I_2 + 2\bar{e} \rightarrow 2I_3^- \quad (2)$$

In this work, we synthesized monometallic and bimetallic MOFs and accomplished their further pyrolysis to form bimetallic nanocarbons.†

The FT-IR spectra of MOF samples and carbon materials were compared to verify changes due to the pyrolysis of MOFs [Figure 1(*a*)]. The characteristic absorption bands corresponding to the asymmetric and symmetric stretching vibrations of benzene-

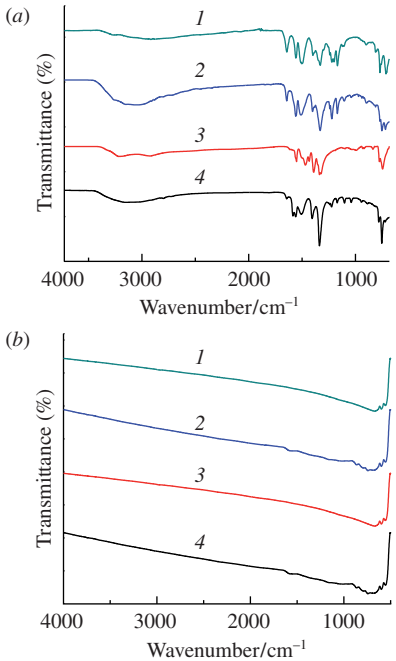

Figure 1 IR spectra of the metal-organic frameworks (*1*) $CuNi_{0.25}$–BTC, (*2*) $CuNi_{0.5}$–BTC, (*3*) Ni–BTC, (*4*) Cu–BTC and metal-containing carbon materials (*1*) $CuNi_{0.25}$@C, (*2*) $CuNi_{0.5}$@C, (*3*) Ni@C, (*4*) Cu@C (*a*) before and (*b*) after pyrolysis.

† Copper(II) nitrate trihydrate (>99.0%), nickel(II) nitrate hexahydrate (>98.0%), ethanol, 1,3,5-benzenetricarboxylic (trimesic) acid (BTC, >95.0%), and sodium hydroxide from Sigma Aldrich were used. A redox electrolyte was composed of 0.1 M $LiCO_4$, 10 mM LiI and 1 mM I_2 solutions in acetonitrile. In the synthesis of MOFs, copper(II) nitrate trihydrate (1.4 g) and trimesic acid (0.75 g) were dissolved in deionized water (20 ml) and ethanol, respectively, in a molar ratio of 2:1; pH 3.5 was adjusted with a 0.1 M solution of NaOH. The $Ni(NO_3)_2$:$Cu(NO_3)_2$ molar ratios were 0, 0.25, 0.5 and 1. The aqueous solution of trimesic acid was added dropwise to the solution of metal salts with stirring at room temperature. The solid precipitates were exposed for 24 h, filtered off and dried at 70 °C for 2 h. The obtained powders were pyrolyzed at 500 °C in an N_2 flow for 2 h. The fabrication of the electrode is described in Online Supplementary Materials.

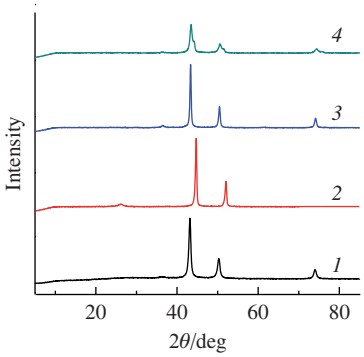

Figure 2 XRD patterns of monometallic (*1*) Cu@C, (*2*) Ni@C and bimetallic (*3*) $CuNi_{0.25}$@C, (*4*) $CuNi_{0.5}$@C carbon materials obtained by pyrolysis at 500 °C.

1,3,5-tricarboxylate (BTC) are in a range of 1620–1373 cm^{-1}. The bands at 3500 and 1200 cm^{-1} are attributed to the vibrations of water molecules linked to metal ions; those at 1050–940 cm^{-1} correspond to the deformed stretching of the carboxylic group owing to coordination with copper ions, while the bands at 910–818 cm^{-1} appeared due to the presence of nickel ions. After the pyrolysis [Figure 1(*b*)], all of the bands disappeared due to the total conversion of mono and bimetallic MOFs into carbon materials. The formed nanocarbon exhibited absorption in a region of 4000 to 400 cm^{-1}.

Figure 2 depicts the XRD patterns of individual M@C and mixed CuNi@C samples. The major XRD peaks of Cu@C at 2θ = 43.25°, 50.21° and 74.02° correspond to the planes (111), (200) and (220), respectively. The very strong peak of carbon at 50.43° indicates a high degree of crystallinity. A peak at 42.93° relates to copper and copper oxide. The peak at 50.43° corresponds to graphitic carbon. Diffraction peaks and planes of $CuNi_{0.5}$@C are similar to those of $CuNi_{0.25}$@C, *viz.*, around 43.42°, 50.43° and 74.14°, which correspond to the (130), (102) and (220) planes, respectively. The strong peak in (130) plane shows a high crystallinity. A small shoulder at 74.02° for $CuNi_{0.5}$@C and $CuNi_{0.25}$@C can be attributed to the presence of nickel in carbon material. The metal moves the peaks to higher 2θ values; both peaks are ascribed to copper–nickel nanoalloy formed during pyrolysis at 500 °C. The high crystallinity of all carbon materials containing metallic copper and copper–nickel alloy was revealed.

The major XRD peaks of Cu-BTC MOFs appeared at 2θ = = 6.9°, 9.4°, 11.56°, 13.41° and 19.17° corresponding to the planes (200), (220), (222), (400) and (333), respectively (Figure S1, see Online Supplementary Materials); this is in agreement with data reported previously.[15] For the Cu–BTC MOF [Figure S1(*a*)], the intensity of peaks indicates a high degree of crystallinity and the absence of copper oxide from the structure (a high material purity). The Ni–BTC MOF exhibited peaks at 2θ = 10.97°, 15.13°, 17.77°, 18.65° and 27.14° corresponding to the (111), (114), (151), (052) and (111) planes, respectively. The strong peaks show a high crystallinity of the material; the peaks do not match with XRD patterns for nickel oxides or hydroxides.

The diffraction peaks for the $CuNi_{0.25}$–BTC and $CuNi_{0.5}$–BTC MOF are similar [Figure S1(*c*),(*d*)], mixed peaks being observed for the copper- and nickel-containing MOFs (the atomic percentages are given in Table S1). The peaks of the bimetallic materials were detected at 2θ = 6.69°, 11.5°, 13.46°, 17.52°, 18.75°, 21.30° and 26.04°, which correspond to the planes (200), (400), (151), (052), (333) and (111), respectively.

In the pyrolyzed MOFs (Figure 2), the signals from the MOFs disappeared and the signs of graphitization appeared in addition to the formation of metal oxide particles. The oxidation of metal cations was caused by the release of water molecules from the BTC MOFs.

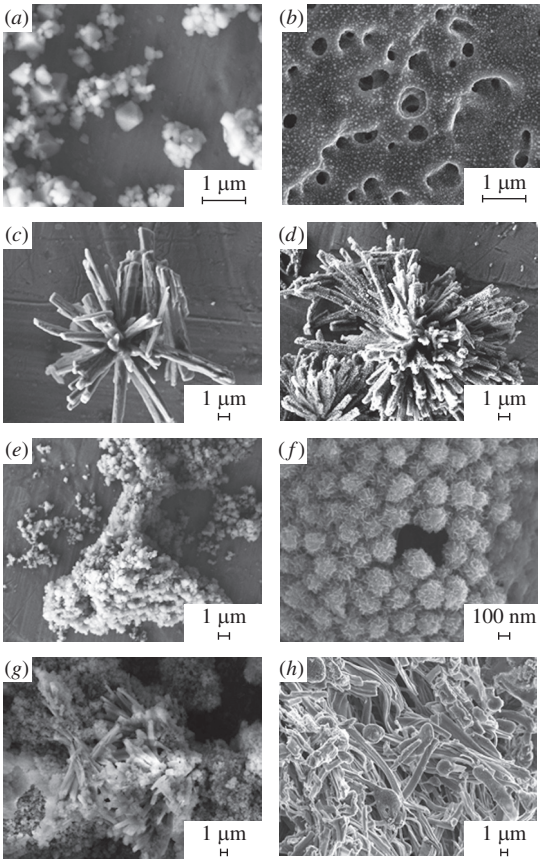

Figure 3 SEM images of (*a*) Cu–BTC, (*b*) Cu@C, (*c*) Ni–BTC, (*d*) Ni@C, (*e*) $CuNi_{0.25}$–BTC, (*f*) $CuNi_{0.25}$@C, (*g*) $CuNi_{0.5}$–BTC, (*h*) $CuNi_{0.5}$@C.

Figure 3 shows the SEM images of individual metal–carbons Cu@C and Ni@C and mixed-metal composites $CuNi_{0.25}$@C and $CuNi_{0.5}$@C. Their morphologies are very different: the copper-containing carbon material had a porous irregular surface [Figure 3(*a*),(*b*)], while a prickle-type morphology was observed in the nickel-containing material [Figure 3(*c*,*d*)]. In both individual copper–carbon [Figure 3(*b*)] and nickel–carbon [Figure 3(*d*)] composites, similar small particles can be seen at the surface of bigger particles or prickles synthesized during the pyrolysis. These are metallic copper and nickel nanoparticles having sizes of 30–50 nm embedded in carbon. Irregular and porous surfaces are favorable for the penetration of electrolyte; thus, a redox reaction on the bimetallic material can occur more quickly. In $CuNi_{0.25}$@C [Figure 3(*f*)], nanoflower-like small particles with incrusted needles can be observed. The particle sizes are around 200 nm with needles of 100 nm. Cavities are formed on the surface with the appearance of a greater active area for catalysis purposes. An irregular morphology is seen in $CuNi_{0.5}$@C [Figure 3(*h*)] containing much bigger needles than those in $CuNi_{0.25}$@C due to the presence of nickel causing changes in the crystal growth. Similarly to individual copper- and nickel-containing materials [see Figure 3(*b*),(*d*)], small particles of 20–35 nm are incrusted on the surface [see Figure 3(*f*),(*h*)]. This irregular morphology increased the contact area between the carbon material and solution, which is favorable for the redox reaction of electrolyte.

Figure 4 shows the CV curves of the counter electrodes with $CuNi_{0.25}$@C and $CuNi_{0.5}$–BTC. The peak current of reduction peak is used to characterize the electrochemical activity of the electrode. Differences between the oxidation and reduction peak potentials for $CuNi_{0.25}$@C, $CuNi_{0.5}$@C, Cu@C and Ni@C are 204, 447, 651 and 751 mV, respectively. Therefore, the potential of $CuNi_{0.25}$@C has a minimum difference, and the reversibility of the electrode is the best among them. The possible reason is the

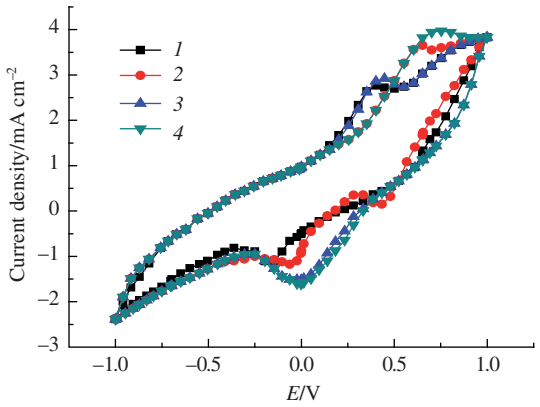

Figure 4 Cyclic voltammograms for (*1*) $CuNi_{0.25}$@C, (*2*) $CuNi_{0.5}$@C, (*3*) Cu@C and (*4*) Ni@C electrodes at a scan rate of 20 mV s^{-1} in 0.1 M $LiClO_4$, 10 mM LiI, 1 mM I_2 solutions in acetonitrile. $LiClO_4$ was used as a supporting electrolyte.

presence of Cu^{2+} and Ni^{2+}, which increase the conductivity of the whole material; in this case, the counter electrode has better catalytic activity and reversibility.

Thus, we successfully synthesized copper–nickel-containing carbon materials by the pyrolysis of metal-organic structures. The bimetallic MOFs were synthesized at room temperature; they can function as electrodes in a redox reaction for the iodine electrolyte. $CuNi_{0.25}$@C and $CuNi_{0.5}$@C have peak potential differences of 204 and 447 mV, respectively, which are lower than that of monometallic carbon materials. These MOFs are potentially applicable to electrodes for the reduction of I_3^- in solar cells.

This work was supported by the CONACyT (Ph.D. scholarship for Cesar M. Oliva González) and the Department of Chemistry of the Universidad Autónoma de Nuevo León (Monterrey, Mexico).

Online Supplementary Materials

Supplementary data associated with this article can be found in the online version at doi: 10.1016/j.mencom.2019.07.014.

References

1 X. Zheng, J. Deng, N. Wang, D. Deng, W. H. Zhang, X. Bao and C. Li, *Angew. Chem., Int. Ed.*, 2014, **53**, 7023.
2 J. I. Feldblyum, E. A. Keenan, A. J. Matzger and S. Maldonado, *J. Phys. Chem. C*, 2012, **116**, 3112.
3 X. Sun, Y. Li, J. Dou, D. Shen and M. Wei, *J. Power Sources*, 2016, **322**, 93.
4 Z. Xie, X. Cui, W. Xu and Y. Wang, *Electrochim. Acta*, 2017, **229**, 361.
5 J. T. Joyce, F. R. Laffir and C. Silien, *J. Phys. Chem. C*, 2013, **117**, 12502.
6 X. Jiang, H. Li, S. Li, S. Huang, C. Zhu and L. Hou, *Chem. Eng. J.*, 2018, **334**, 419.
7 B. Huskinson, M. P. Marshak, C. Suh, S. Er, M. R. Gerhardt, C. J. Galvin, X. Chen, A. Aspuru-Guzik, R. G. Gordon and M. J. Aziz, *Nature*, 2014, **505**, 195.
8 G. Yu, J. Gao, J. C. Hummelen, F. Wudl and A. J. Heeger, *Science*, 1995, **270**, 1789.
9 E. Kymakis and G. A. J. Amaratunga, *Appl. Phys. Lett.*, 2002, **80**, 112.
10 P. Avouris, M. Freitag and V. Perebeinos, *Nat. Photonics*, 2008, **2**, 341.
11 P. V. Kamat, M. Haria and S. Hotchandani, *J. Phys. Chem.*, 2004, **108**, 5166.
12 E. Ramasamy, W. J. Lee, D. Y. Lee and J. S. Song, *Electrochem. Commun.*, 2008, **10**, 1087.
13 P. J. Kulesza, J. K. Zak, I. A. Rutkowska, B. Dembinska, S. Zoladek, K. Miecznikowski, E. Negro, V. Di Noto and P. Zelenay, *Curr. Opin. Electrochem.*, 2018, **9**, 257.
14 Y. Li, C. Chen, X. Sun, J. Dou and M. Wei, *ChemSusChem*, 2014, **7**, 2469.
15 S. Najafi Nobar, *Mater. Chem. Phys.*, 2018, **213**, 343.
16 K. Cui and S. Maruyama, *Prog. Energy Combust. Sci.*, 2019, **70**, 1.
17 A. Aqel, K. M. M. Abou El-Nour, R. A. A. Ammar and A. Al-Warthan, *Arab. J. Chem.*, 2012, **5**, 1.
18 J. Qiu, X. Zhang, Y. Feng, X. Zhang, H. Wang and J. Yao, *Appl. Catal., B*, 2018, **231**, 317.
19 A. Banerjee, K. E. Halvorsen, A. Eastmond-Spencer and S. R. Sweitz, *Environ. Manage.*, 2017, **59**, 912.
20 A. Kay and M. Grätzel, *Sol. Energy Mater. Sol. Cells*, 1996, **44**, 99.
21 S. Venkatesan and Y.-L. Lee, *Coord. Chem. Rev.*, 2017, **353**, 58.
22 D. A. Stewart and F. Léonard, *Nano Lett.*, 2005, **5**, 219.
23 L. Kavan, J.-H. Yum and M. Grätzel, *Nano Lett.*, 2011, **11**, 5501.
24 D. Y. Lee, D. V. Shinde, S. J. Yoon, K. N. Cho, W. Lee, N. K. Shrestha and S.-H. Han, *J. Phys. Chem. C*, 2014, **118**, 16328.

Received: 7th March 2019; Com. 19/5848